Imbalanced nucleocytoskeletal connections create common polarity defects in progeria and physiological aging

Wakam Chang[a], Yuexia Wang[a,b], G. W. Gant Luxton[a,1], Cecilia Östlund[a,b], Howard J. Worman[a,b], and Gregg G. Gundersen[a,2]

[a]Department of Pathology and Cell Biology, Vagelos College of Physicians and Surgeons, Columbia University, New York, NY 10032; and [b]Department of Medicine, Vagelos College of Physicians and Surgeons, Columbia University, New York, NY 10032

Edited by Daniel A. Starr, University of California, Davis, CA, and accepted by Editorial Board Member Sue Biggins January 7, 2019 (received for review June 5, 2018)

Studies of the accelerated aging disorder Hutchinson–Gilford progeria syndrome (HGPS) can potentially reveal cellular defects associated with physiological aging. HGPS results from expression and abnormal nuclear envelope association of a farnesylated, truncated variant of prelamin A called "progerin." We surveyed the diffusional mobilities of nuclear membrane proteins to identify proximal effects of progerin expression. The mobilities of three proteins—SUN2, nesprin-2G, and emerin—were reduced in fibroblasts from children with HGPS compared with those in normal fibroblasts. These proteins function together in nuclear movement and centrosome orientation in fibroblasts polarizing for migration. Both processes were impaired in fibroblasts from children with HGPS and in NIH 3T3 fibroblasts expressing progerin, but were restored by inhibiting protein farnesylation. Progerin affected both the coupling of the nucleus to actin cables and the oriented flow of the cables necessary for nuclear movement and centrosome orientation. Progerin overexpression increased levels of SUN1, which couples the nucleus to microtubules through nesprin-2G and dynein, and microtubule association with the nucleus. Reducing microtubule-nuclear connections through SUN1 depletion or dynein inhibition rescued the polarity defects. Nuclear movement and centrosome orientation were also defective in fibroblasts from normal individuals over 60 y, and both defects were rescued by reducing the increased level of SUN1 in these cells or inhibiting dynein. Our results identify imbalanced nuclear engagement of the cytoskeleton (microtubules: high; actin filaments: low) as the basis for intrinsic cell polarity defects in HGPS and physiological aging and suggest that rebalancing the connections can ameliorate the defects.

Hutchinson–Gilford progeria syndrome | SUN proteins | LINC complex | nuclear movement | centrosome orientation

Hutchinson–Gilford progeria syndrome (HGPS) is an accelerated aging syndrome caused by mutations in *LMNA* encoding prelamin A and lamin C (1, 2). In normal cells, prelamin A undergoes a series of modifications to produce mature lamin A. The C-terminal CaaX motif of prelamin A is farnesylated, followed by C-terminal methylation and removal of the last three amino acids, and a final cleavage that removes another 15 amino acids of the C terminus including the farnesylated cysteine (3). In HGPS, a cryptic splice site in prelamin A mRNA is activated, resulting in the production of a truncated variant, termed "progerin," which lacks the final cleavage site and remains farnesylated (1, 2). By retaining its farnesyl moiety, progerin accumulates on the inner nuclear membrane where it affects nuclear architecture and functions associated with the nuclear lamina (4–6). Progerin expression causes nuclear shape abnormalities and alters many nuclear functions and cellular pathways (4, 7–9). In most cases, how progerin expression leads to these alterations is poorly understood.

Most studies have attributed alterations caused by progerin to its effects on the lamina. However, because progerin associates with the inner nuclear membrane, it may also dominantly interfere with other nuclear envelope proteins (10). Lamin A plays a critical role in the function of the linker of nucleoskeleton and cytoskeleton (LINC) complex. This complex is composed of inner nuclear membrane SUN proteins and outer nuclear membrane KASH proteins (known as nesprins in vertebrates) (11, 12). Through interaction of nesprins with the cytoskeleton, the LINC complex contributes to nuclear movement and positioning, organization of the cytoskeleton, mechanotransduction to the nucleus, DNA repair, and meiotic chromosome movements (11–16). Lamin A interacts with both SUN1 and SUN2, the major SUN domain proteins in somatic cells. Although it is not critical for their nuclear localization, it affects their mobilities and lack of lamin A prevents the anchoring of the LINC complex that is necessary for transmitting force (17–19).

There are few studies of the effects of progerin on the cellular functions of the LINC complex. Progerin, like farnesylated prelamin A, exhibits increased association with SUN1 compared with SUN2 (17, 20). This may explain the increased levels of SUN1 observed in fibroblasts from children with HGPS and is likely to have deleterious physiological consequences as skeletal

Significance

The rare, premature aging syndrome Hutchinson–Gilford progeria syndrome (HGPS) arises from expression of a pathological prelamin A variant, termed "progerin." Studies of progerin may identify treatments for HGPS and reveal novel cellular and molecular characteristics of normal aging. Here, we show that progerin selectively affects mobilities of three nuclear membrane proteins—SUN2, nesprin-2G, and emerin—that position the nucleus and establish cell polarity essential for migration. We find that both processes are defective in fibroblasts from children with HGPS and aged (>60 y) individuals. The mechanism underlying these defects is excessive interaction of the nucleus with microtubules. Our work identifies nuclear-based defects in cell polarization as intrinsic factors in premature and physiological aging and suggests a means for correcting them.

Author contributions: W.C., Y.W., G.W.G.L., C.Ö., H.J.W., and G.G.G. designed research; W.C., Y.W., G.W.G.L., and C.Ö. performed research; W.C. contributed new reagents/analytic tools; W.C., Y.W., G.W.G.L., C.Ö., H.J.W., and G.G.G. analyzed data; and W.C., H.J.W., and G.G.G. wrote the paper.

The authors declare no conflict of interest.

This article is a PNAS Direct Submission. D.A.S. is a guest editor invited by the Editorial Board.

[1]Present address: Department of Genetics, Cell Biology, and Development, University of Minnesota, Minneapolis, MN 55455.

[2]To whom correspondence should be addressed. Email: ggg1@cumc.columbia.edu.

This article contains supporting information online at www.pnas.org/lookup/suppl/doi:10.1073/pnas.1809683116/-/DCSupplemental.

Published online February 11, 2019.

phenotypes and shortened life span of progeroid mouse models are improved by knocking out SUN1 (21). In homeostatic positioning of nuclei, SUN1 and SUN2 function separately to support nesprin-2G coupling to microtubules and actin filaments, respectively, and overexpressing one of the SUN proteins interferes with the function of the other ("transdominant inhibition") (22). Thus, the up-regulation of SUN1 in fibroblasts from individuals with HGPS may itself alter LINC complex function.

Here, we explore the hypothesis that progerin expression alters nuclear membrane proteins through its association with the inner nuclear membrane. We identify a subset of nuclear membrane proteins that are altered by progerin expression and show that their function in nuclear movement and cell polarity is disrupted. We find similar defects in fibroblasts from aged individuals and identify excessive microtubule interactions with the nucleus as the cause in fibroblasts from both HGPS and aged individuals.

Results

Progerin Expression Reduces the Diffusional Mobilities of Selected Nuclear Membrane Proteins. We surveyed the diffusional mobilities of EGFP-tagged integral nuclear membrane proteins by fluorescence recovery after photobleaching (FRAP) in fibroblasts from children with HGPS (HGPS fibroblasts) and age- and sex-matched controls (*SI Appendix*, Table S1). We tested proteins that interact directly or indirectly with lamins A and C (lamin A/C), including emerin, lamina-associated polypeptide 1 (LAP1), and LINC complex proteins (12, 23, 24). This survey revealed that the mobilities of mini–nesprin-2G (mN2G), a truncated form of nesprin-2G that functionally supports actin-dependent nuclear movement (25), SUN2, and emerin, but not five other nuclear membrane proteins (nesprin-3α, nesprin-3β, nesprin-4, SUN1, or LAP1), were significantly reduced in fibroblasts from individuals with HGPS compared with those from unaffected controls (Fig. 1*A* and *SI Appendix*, Fig. S1 *A* and *B*). In HGPS fibroblasts from four different individuals, the half-times of recovery ($t_{1/2}$) of mN2G and SUN2 were consistently longer than those in control fibroblasts (*SI Appendix*, Fig. S1*C*). We did not detect a reduction in the mobility of SUN1, previously reported in HeLa cells overexpressing progerin (20), in all four HGPS fibroblast samples that we tested (*SI Appendix*, Fig. S1*C*). Despite their altered diffusional mobilities, the nuclear localizations of nesprin-2G, SUN2, and emerin appeared similar in HGPS and control fibroblasts (*SI Appendix*, Fig. S2*A*).

We next tested whether progerin was responsible for the altered mobilities. Treatment of HGPS fibroblasts with the protein farnesyltransferase inhibitor (FTI 277) at a concentration that blocked prelamin A processing (*SI Appendix*, Fig. S2*B*) significantly increased the diffusional mobilities and decreased the $t_{1/2}$ of EGFP-tagged mN2G, SUN2, and emerin in HGPS fibroblasts without affecting their baseline mobilities in normal fibroblasts (Fig. 1*B* and *SI Appendix*, Fig. S1*D*). SUN protein levels were not affected by FTI treatment (*SI Appendix*, Fig. S2*C*). Ectopic expression of RFP-progerin in NIH 3T3 fibroblasts also reduced the diffusional mobilities of mN2G and SUN2 (Fig. 1*C* and *SI Appendix*, Fig. S1*E*). Thus, progerin farnesylation was necessary, and progerin expression was sufficient to reduce the diffusional mobilities of mN2G and SUN2.

Progerin Expression Causes Polarity Defects in Migratory Fibroblasts. Nesprin-2G, SUN2, and emerin are all required for rearward nuclear movement and centrosome positioning in fibroblasts and myoblasts polarizing for migration (25–27), which is known to be impaired by HGPS (7, 28). After stimulation with serum or the serum factor lysophosphatidic acid (LPA), nesprin-2G and SUN2 assemble into transmembrane actin-associated nuclear (TAN) lines that couple the nucleus to perinuclear actin cables to move it to the cell rear, resulting in centrosome orientation (25, 29). In contrast, emerin interacts with myosin-IIB on the outer nuclear membrane to orient the flow of perinuclear actin cables (26). In LPA-stimulated HGPS fibroblasts, rearward nuclear positioning was impaired, preventing proper centrosome orientation; however, these processes were restored by treatment with FTI 277 (Fig. 2 *A*–*C*). To test if progerin was directly responsible for these defects, we expressed EGFP-tagged lamin A variants in NIH 3T3 fibroblasts. Expression of EGFP-tagged progerin—but not of wild-type lamin A or a nonfarnesylatable progerin variant the carboxyl-terminal Cys-Ser-Ile-Met motif of which was mutated to Ser-Ser-Ile-Met (SSIM) (30)—inhibited rearward nuclear positioning and centrosome orientation (Fig. 2 *D*–*F*). Treatment with FTI 277 reversed the effects of EGFP-progerin but had no effects in cells expressing EGFP-lamin A (Fig. 2 *D*–*F*). Thus, farnesylated progerin inhibits the acquisition of polarity in fibroblasts by preventing rearward nuclear positioning.

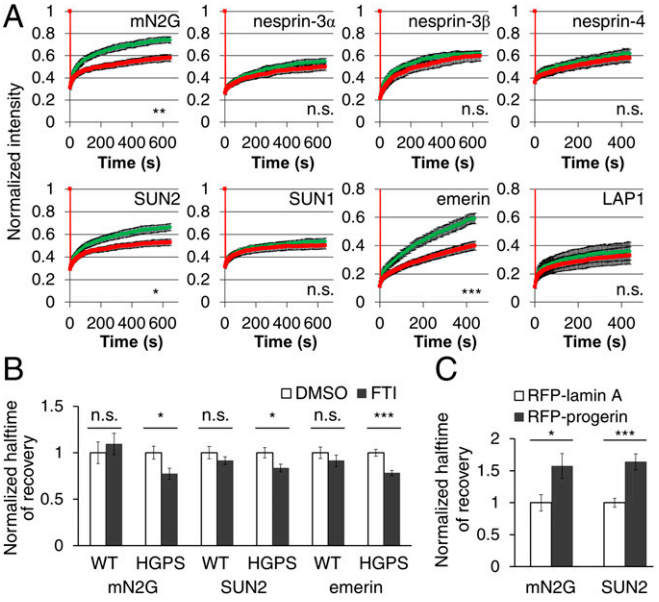

Fig. 1. Progerin expression reduces the diffusional mobilities of a subset of nuclear envelope proteins. (*A*) Normalized FRAP in the nuclear envelope for indicated EGFP-tagged proteins in control (WT, green) and HGPS fibroblasts (red). The $t_{1/2}$ of FRAP are used for statistical tests. (*B*) Normalized $t_{1/2}$ of FRAP of EGFP-tagged mN2G, SUN2, and emerin in HGPS fibroblasts treated with 2.5 μM FTI 277. Values are normalized to cells treated with dimethyl sulfoxide (DMSO). (*C*) Normalized $t_{1/2}$ of FRAP of EGFP-tagged mN2G and SUN2 in NIH 3T3 fibroblasts expressing RFP-tagged lamin A or progerin. See *SI Appendix*, Table S2, for absolute numbers for $t_{1/2}$. Data are mean ± SEM from ≥3 experiments (n > 15 cells). n.s., P > 0.05; *P < 0.05; **P < 0.01; ***P < 0.001 by Student's t test.

Progerin Expression Affects TAN Line Anchorage and Actin Retrograde Flow. To determine how progerin affects nuclear positioning in HGPS fibroblasts, we examined TAN line assembly and actin retrograde flow. TAN lines, which are identified by the accumulation of EGFP-mN2G and endogenous SUN2 along perinuclear actin cables on the dorsal nuclear surface (25), formed similarly in HGPS and control fibroblasts (Fig. 3 *A*–*C*). However, live cell imaging revealed that TAN lines in cells expressing EGFP-progerin moved rearward, albeit slowly (see Fig. 3 *F* and *G* below), on immobile nuclei (Fig. 3*C* and Movie S1). This slippage of TAN lines indicated that they are not strongly anchored in these cells, a phenotype similar to that occurring in fibroblasts lacking lamin A/C (19).

Expression of EGFP-progerin also affected the retrograde flow of actin near the leading edge. As previously reported (19, 25), in control NIH 3T3 fibroblasts and those expressing EGFP-lamin A, actin cables near the leading edge exhibited predominantly

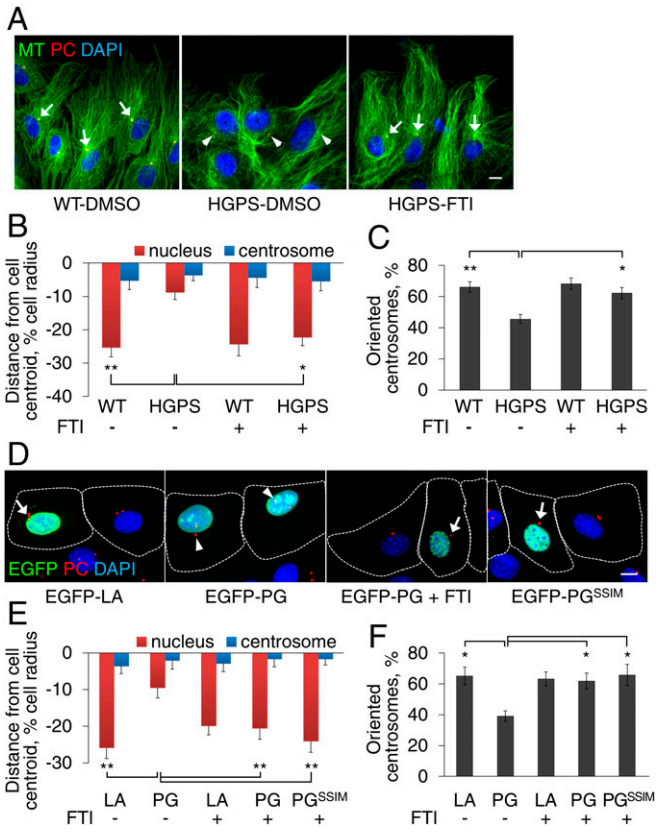

Fig. 2. Progerin expression causes polarity defects in migratory fibroblasts. (*A*) Representative images of microtubules (MT), centrosomes [pericentrin (PC)], and nuclei (DAPI) in LPA-stimulated control (WT) and HGPS fibroblasts pretreated with vehicle (DMSO) or FTI 277. Arrows: oriented centrosomes; arrowheads: nonoriented centrosomes. (*B*) Quantification of nuclear (red) and centrosomal (blue) positions along the front–back axis of LPA-stimulated WT or HGPS fibroblasts treated with or without FTI 277. The cell centroid is defined as "0"; plus (+) values: toward the leading edge; minus (–) values: toward the cell rear. (*C*) Quantification of centrosome orientation for the cells treated as in *B*. Random centrosome orientation is 33%. (*D*) Representative images of LPA-stimulated NIH 3T3 fibroblasts transiently expressing EGFP-tagged lamin A (LA), progerin (PG, ±FTI treatment), or a nonfarnesylatable progerin variant (PG^{SSIM}). Dashed lines indicate cell outlines; arrows and arrowheads are as in *A*. (*E* and *F*) Quantification of nuclear and centrosomal positions (*E*) and centrosome orientation (*F*) in LPA-stimulated NIH 3T3 fibroblasts cells expressing the indicated EGFP-tagged constructs treated with or without FTI 277. Data are mean ± SEM from ≥3 experiments ($n > 90$ cells per experiment). $^*P < 0.05$ and $^{**}P < 0.01$ by *t* test. (Scale bars, *A* and *D*: 10 μm.)

rearward movement at a rate of 0.28 ± 0.05 μm/min (Fig. 3 *E* and *G* and Movie S2). In contrast, in cells expressing EGFP-progerin the velocity was only 0.05 ± 0.02 μm/min (Fig. 3 *F* and *G* and Movie S3). The velocity of actin cables in cells expressing a nonfarnesylatable progerin variant was 0.30 ± 0.05 μm/min (Fig. 3*G*). Actin cables in cells expressing EGFP-progerin also exhibited significantly more nondirectional actin flow compared with cells expressing EGFP-lamin A (Fig. 3*H*). Thus, farnesylated progerin affects rearward nuclear movement by both weakening TAN line anchorage and disturbing retrograde actin flow.

Cell Polarity Defects in HGPS Are Mediated by Increased SUN1. The defects in TAN line anchorage and actin retrograde flow in progerin-overexpressing cells are reminiscent of those in lamin A/C-deficient cells (19) and emerin-deficient cells (26), respectively. How does progerin affect both these processes? We considered the possibility that the up-regulation of SUN1 observed with progerin overexpression (21) may exert a transdominant inhibitory effect preventing SUN2-nesprin-2G coupling to the actin cytoskeleton (22). We confirmed the previously reported up-regulation of SUN1 in HGPS fibroblasts (21) and additionally found that stable expression of progerin, but not of lamin A, in NIH 3T3 fibroblasts proportionately increased the level of SUN1 but not of SUN2 in the nucleus (Fig. 4 *A* and *B*). This shows that progerin overexpression specifically increases SUN1 levels and is consistent with earlier reports that the levels of SUN1 and SUN2 are not interdependent (22, 25). These findings suggest that an elevated level of SUN1 may contribute to the nuclear movement and cell polarity defects in HGPS fibroblasts. Indeed, stable overexpression of

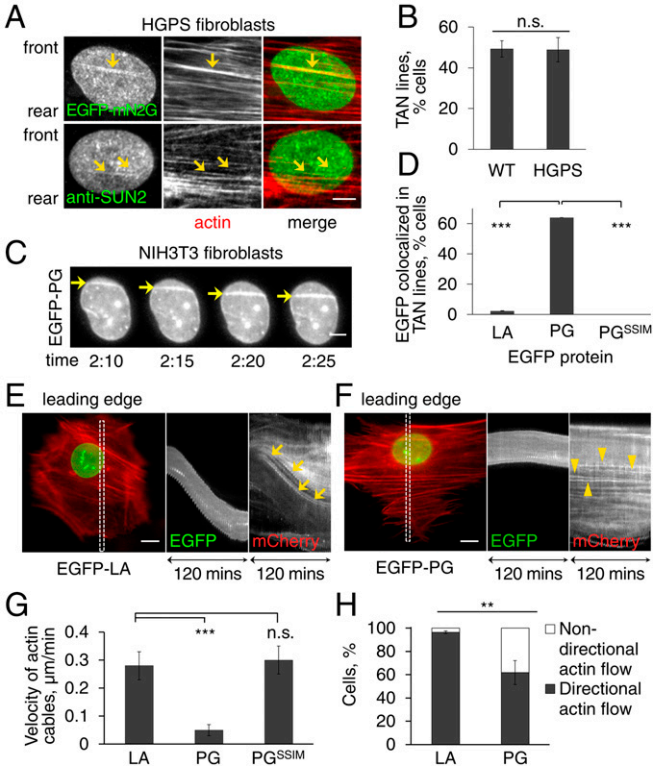

Fig. 3. Progerin expression affects TAN line anchorage to the nuclear envelope and retrograde actin flow. (*A*) Representative images of a nucleus in an LPA-stimulated HGPS fibroblast expressing EGFP-mN2G (*Top*) or stained for SUN2 (*Bottom*). mN2G and SUN2 formed linear structures (arrows) that colocalized with actin filaments (stained by phalloidin) indicating TAN line formation. (*B*) Quantification of TAN line formation in control (WT) and HGPS fibroblasts ($n = 3$ experiments; $n > 70$ cells). (*C*) Images from a movie (Movie S1) of EGFP-progerin in NIH 3T3 fibroblasts. Note accumulation of EGFP-progerin in TAN lines (arrows) that slip over an immobile nucleus. (See Movie S1 for mCherry-LifeAct signal.) Time, h:min after LPA treatment. (*D*) Quantification of cells in which the indicated EGFP-tagged proteins (LA, lamin A; PG, progerin) colocalized with TAN lines ($n = 3$ experiments; $n > 50$ cells). (*E* and *F*) Representative kymographs from movies of LPA-stimulated NIH 3T3 fibroblasts expressing EGFP-lamin A (LA) (*E*, from Movie S2) or EGFP-progerin (PG) (*F*, from Movie S3) together with mCherry-LifeAct. The color image is the first frame of the movies (30 min after LPA stimulation) and shows the region (box) used for the kymographs on the *Right*. Note slower rearward actin flow in cells expressing EGFP-progerin (arrowheads) compared with EGFP-lamin A (arrows). Leading edge of the cells is toward the top in all panels. (*G*) Quantification of the velocity of retrograde actin flow near the leading edge in NIH 3T3 fibroblasts expressing mCherry-LifeAct and the indicated EGFP-tagged proteins (LA, lamin A; PG, progerin) ($n = 3$ experiments, $n > 40$ actin cables). (*H*) Quantification of the directionality of actin flow in NIH 3T3 fibroblasts expressing mCherry-LifeAct and indicated EGFP-tagged proteins (LA, lamin A; PG, progerin) ($n = 3$ experiments; $n > 50$ cells). Data are mean ± SEM from ≥3 experiments. n.s., $P > 0.05$; $^{**}P < 0.01$; $^{***}P < 0.001$ by *t* test. (Scale bars, *A* and *C*: 5 μm; *E* and *F*: 10 μm.)

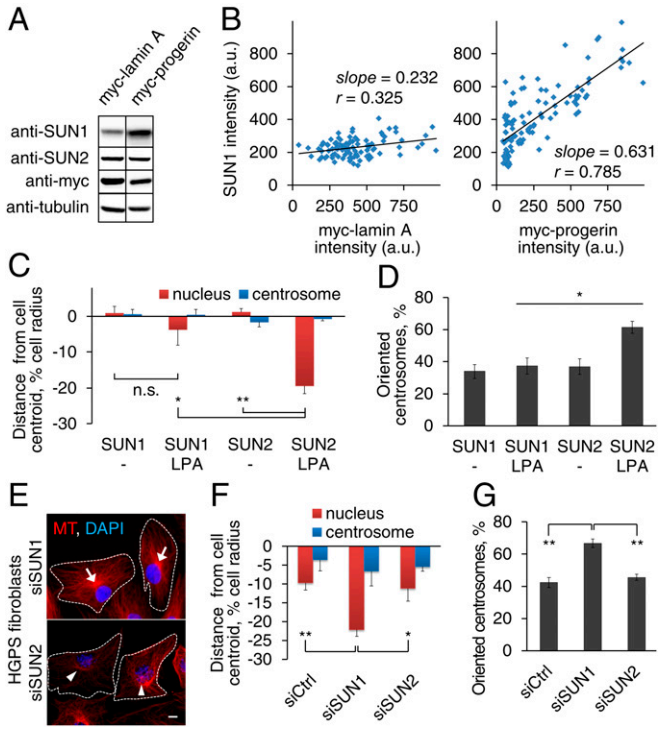

Fig. 4. Cell polarity defects in HGPS fibroblasts are mediated by increased SUN1. (*A*) Immunoblot of lysates from myc-lamin A or progerin expressing NIH 3T3 fibroblasts probed with the indicated antibodies. Tubulin is a loading control. (*B*) Quantification of signal intensities in individual NIH 3T3 fibroblasts ($n > 120$) stably expressing myc-tagged lamin A (*Left*) or progerin (*Right*) and stained for myc and SUN1. Correlation coefficients (r) and slopes were calculated assuming a linear relationship. (*C* and *D*) Quantification of nuclear and centrosomal positions (*C*) and centrosome orientation (*D*) in NIH 3T3 fibroblasts stably expressing myc-SUN1 or myc-SUN2 and treated with or without LPA. (*E*) Representative images of microtubules (MT) and nuclei (DAPI) in LPA-stimulated HGPS fibroblasts treated with indicated siRNAs. Arrows: oriented centrosomes; arrowheads: nonoriented centrosomes; dashed lines: cell borders. (Scale bar, 10 μm.) (*F* and *G*) Quantification of nuclear and centrosomal positions (*F*) and centrosome orientation (*G*) in LPA-stimulated HGPS fibroblasts treated with indicated siRNAs. Data are mean ± SEM from ≥ 3 experiments ($n > 90$ cells). n.s., $P > 0.05$; *$P < 0.05$; and **$P < 0.01$ by t test.

SUN1 in NIH 3T3 fibroblasts prevented rearward nuclear movement and centrosome orientation (Fig. 4 *C* and *D*). Critically, SUN1 depletion by siRNA treatment (*SI Appendix*, Fig. S3*A*) rescued the defects in rearward nuclear movement and centrosome orientation in HGPS fibroblasts (Fig. 4 *E*–*G*). As with FTI 277 treatment, SUN1 depletion from HGPS fibroblasts significantly increased the diffusional mobility of EGFP-mN2G (*SI Appendix*, Fig. S3 *B* and *C*). These results indicate that elevated SUN1 expression is responsible for the cell polarity defects in HGPS fibroblasts.

Cell Polarity Defects in HGPS Fibroblasts Are Mediated by the Microtubule Cytoskeleton. SUN1 and SUN2 are ubiquitously expressed in somatic cells but separately support nesprin-2G–dependent nuclear movement by microtubules and actin filaments, respectively (22). Additionally, overexpression of one SUN protein transdominantly inhibits the ability of the other to support nuclear movement (Fig. 4*C* and ref. 22). The elevated levels of SUN1 and the rescue of actin- and SUN2-dependent rearward nuclear positioning by SUN1 depletion suggested that the nucleus in HGPS fibroblasts may interact abnormally with microtubules. Indeed, we observed excessive association of microtubules with nuclei in HGPS fibroblasts compared with control fibroblasts (Fig. 5*A*). To directly test if microtubules contribute to polarity defects in HGPS fibroblasts, we used a dynein inhibitor, HPI-4 (ciliobrevin A), which inhibits SUN1- and microtubule-dependent nuclear movement in fibroblasts (22). At a low concentration, HPI-4 did not improve nuclear morphology but rescued actin-dependent nuclear movement in both HGPS fibroblasts (Fig. 5 *B* and *C*) and NIH 3T3 fibroblasts overexpressing progerin (Fig. 5 *E* and *F*). HPI-4 also increased centrosome orientation (Fig. 5 *D* and *G*), even though it caused the centrosome to move rearward with the nucleus as expected, given dynein's role in maintaining the centrosome in the cell center (29). HPI-4 treatment did not affect SUN levels and did not rescue the mobilities of mN2G and SUN2 (*SI Appendix*, Fig. S3 *D*–*F*), suggesting that the bulk mobility of these proteins is determined by their nuclear anchorage rather than by their cytoskeletal interactions.

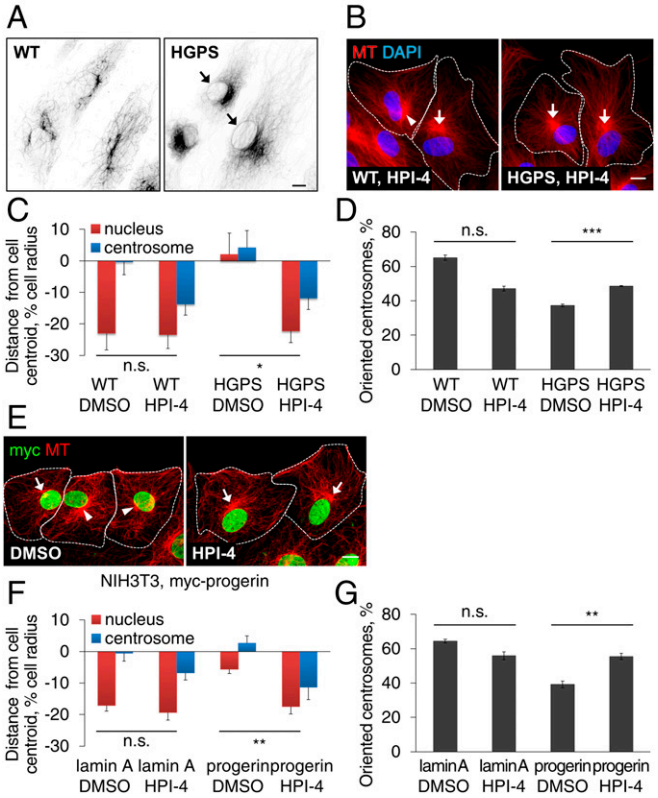

Fig. 5. Cell polarity defects in HGPS fibroblasts are mediated by the microtubule cytoskeleton. (*A*) Representative images of microtubules (MT) and nuclei (DAPI) in WT (*Left*) and HGPS (*Right*) fibroblasts treated with 10 μM nocodazole for 2 h. Inverted contrast is shown. Nocodazole-resistant microtubules surrounding nuclei (arrows) were observed more frequently in HGPS fibroblasts (29.5%, $n = 670$ cells, $n = 2$) compared with WT fibroblasts (0.20%, $n = 1000$ cells, $n = 2$). (*B*) Representative images of microtubules (MT) and nuclei (DAPI) in WT (*Left*) and HGPS (*Right*) fibroblasts pretreated with 5 μM HPI-4 for 1 h and stimulated with LPA. Arrows: oriented centrosomes; arrowheads, unoriented centrosomes; dashed lines, cell borders. (*C* and *D*) Quantification of nuclear and centrosomal positions (*C*) and centrosome orientation (*D*) in LPA-stimulated WT and HGPS fibroblasts pretreated with vehicle (DMSO) or 5 μM HPI-4 for 1 h. (*E*) Images of microtubules (MT) and myc-progerin in NIH 3T3 fibroblasts stably expressing myc-progerin and treated with DMSO or 10 μM HPI-4 for 1 h before LPA stimulation. Arrows, arrowheads, and dashed lines are as in *B*. (*F* and *G*) Quantification of nuclear and centrosome positions (*F*) and centrosome orientation (*G*) in LPA-stimulated NIH 3T3 fibroblasts expressing myc-tagged lamin A or progerin and pretreated with either DMSO or 10 μM HPI-4 for 1 h. Data are mean ± SEM from ≥ 3 experiments ($n > 90$ cells). n.s., $P > 0.05$; *$P < 0.05$; **$P < 0.01$; and ***$P < 0.001$ by t test. (Scale bars, *A*, *B*, and *E*: 10 μm.)

Fibroblasts from Aged Individuals Exhibit Similar Nuclear Movement and Cell Polarity Defects as HGPS Fibroblasts. As in HGPS (7, 28), nuclear architecture and cell migration are altered by physiological aging (5, 31, 32), but whether cell polarity is affected in aged migratory cells is unknown. We therefore examined centrosome orientation and nuclear movement in fibroblasts of comparable early passages from young (3–10 y old) and aged (87–90 y old) human males. Rearward nuclear movement and centrosome orientation stimulated by LPA occurred in fibroblasts from young but not aged individuals (Fig. 6 *A*–*C*). To determine the age at which centrosome orientation becomes defective, we examined fibroblasts from a broader range of ages (*SI Appendix*, Tables S4 and S5). Centrosome orientation was normal in fibroblasts from both male and female subjects up to 60 y of age but was impaired in fibroblasts from virtually all those older than 60 y (Fig. 6*D*).

The inability of cells from aged individuals to polarize did not reflect a general defect in LPA-mediated signaling, as LPA stimulated the assembly of actin stress fibers in these cells (Fig. 6*A*), one of the canonical responses to LPA (33). These polarity defects did not correlate with dysmorphic nuclei (found in 6.9% of young and 8.7% of aged cells; ≥600 cells; $P > 0.05$ by χ^2 test), proliferation (*SI Appendix*, Fig. S4*A*), or cellular senescence (*SI Appendix*, Fig. S4 *B* and *C*), factors associated with aged cells as they are cultured for prolonged times (34). They also did not correlate with age- and passage-associated accumulation of DNA damage measured by phosphorylated H2AX (*SI Appendix*, Fig. S4*D*) (35). Additionally, although fibroblasts from young individuals accumulated markers of cellular senescence at later passages (*SI Appendix*, Fig. S4*C*), centrosome orientation in these cells was normal (*SI Appendix*, Fig. S4*E*). These results indicate that defects in nuclear movement and polarization are cell intrinsic phenotypes common to accelerated and physiological aging and are independent of other markers of cellular aging.

Cell Polarity Defects in Fibroblasts from Aged Individuals Are Rescued by Reducing Microtubule Coupling to the Nucleus. We detected progerin expression at low levels in fibroblasts from both young and aged individuals, but similar to a previous report, we did not detect a consistent difference between the samples (*SI Appendix*, Fig. S5). We next checked whether SUN1 was up-regulated in fibroblasts from aged individuals as in HGPS fibroblasts. In whole-cell lysates of fibroblasts from aged individuals, SUN1 expression was significantly elevated compared with lysates from fibroblasts from young individuals (Fig. 6*E*). These results suggested that the polarity defects in aged cells may have the same mechanistic basis as in the HGPS fibroblasts. Indeed, knockdown of SUN1 (but not SUN2) rescued the polarity defects in aged fibroblasts (Fig. 6 *F* and *G*). Similarly, HPI-4 treatment restored nuclear movement and partially rescued centrosome orientation (Fig. 6 *H* and *I*). These results indicate that elevated SUN1 expression is responsible for the cell polarity defects in fibroblasts from children with HGPS and physiologically aged individuals.

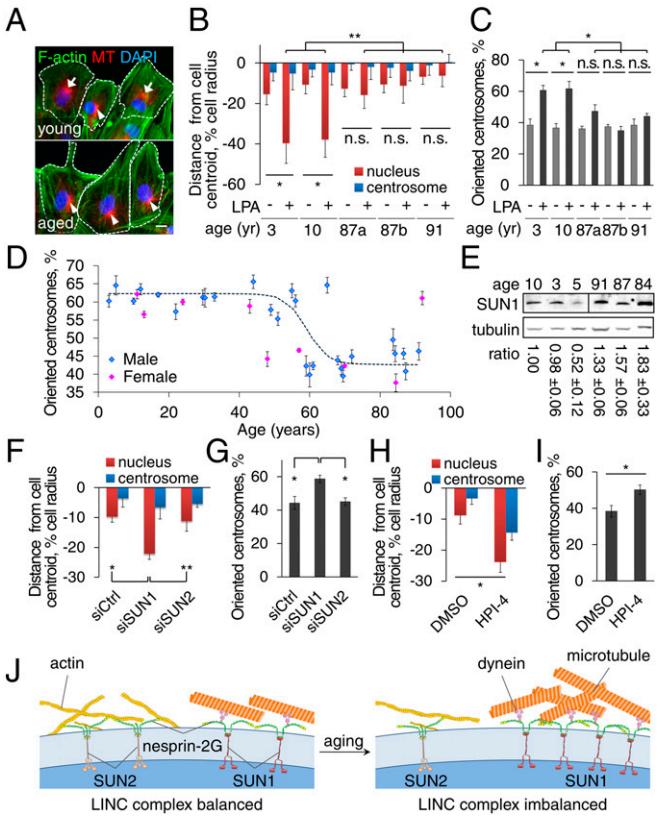

Fig. 6. Fibroblasts from aged individuals exhibit cell polarity defects that are ameliorated by SUN1 knockdown and dynein inhibitor. (*A*) Representative images of F-actin, microtubules (MT), and nuclei (DAPI) in LPA-stimulated fibroblasts from young (10 y) and aged (87 y) male individuals. Arrows: oriented centrosomes; arrowheads: unoriented centrosomes; dashed lines: cell borders. (Scale bar, 10 μm.) (*B* and *C*) Quantification of nuclear and centrosomal positions (*B*) and centrosome orientation (*C*) in LPA-stimulated fibroblasts from young and aged male individuals (87a and 87b are different individuals). (*D*) Quantification of centrosome orientation after LPA stimulation of fibroblasts from males (blue) and females (pink) of different ages. The trend line is a logistic regression curve fitted to the results for male fibroblasts ($P < 0.0001$, Pearson's χ^2 test). (*E*) Immunoblots of SUN1 and tubulin in fibroblasts from young and aged individuals. The SUN1/tubulin ratio is mean ± SEM from three experiments and is normalized to the leftmost sample ($P < 0.05$ by t test, young versus aged cells). (*F* and *G*) Quantification of nuclear and centrosomal positions (*F*) and centrosome orientation (*G*) in LPA-stimulated fibroblasts (87 y) treated with indicated siRNAs. (*H* and *I*) Quantification of nuclear and centrosome positions (*H*) and centrosome orientation (*I*) in LPA-stimulated aged (87 y) fibroblasts treated with vehicle (DMSO) or 5 μM HPI-4 for 1 h. Data are mean ± SEM from ≥ 3 experiments ($n > 90$ cells). n.s., $P > 0.05$; *$P < 0.05$; **$P < 0.01$ by t test. (*J*) Model for the imbalanced engagement of the nucleus with the cytoskeleton in fibroblasts from HGPS and aged individuals.

Discussion

Establishing and maintaining polarity are essential for many cellular functions, including productive migration, which is critical for tissue renewal and repair (36). Reduced cell migration is an aging phenotype and has been proposed to contribute to some of the symptoms of HGPS (7, 28, 31, 32). Here we show that, in fibroblasts from HGPS and aged individuals, nuclear engagement with microtubules is favored compared with actin filaments, leading to an imbalance in the two systems and defects in cell polarization (Fig. 6*J*).

Our data suggest that the primary effect of progerin on actin-dependent nuclear movement and cell polarization is mediated by increased SUN1 levels. Elevated progerin expression increases SUN1 accumulation, most likely because of SUN1's propensity to interact strongly with it (20). Elevated SUN1 is likely to have two consequences on actin-dependent nuclear movement. First, the preference of SUN1-nesprin-2G LINC complexes for microtubules (22) would make it more difficult for the nucleus to be moved by actin filaments. This would produce slipping TAN lines not because of an inability for them to be anchored as in lamin A null cells (19), but because the nucleus itself is excessively anchored. Consistent with this conclusion, we observed normal actin-dependent nuclear movement by both reducing SUN1 levels and by inhibiting dynein. Elevated SUN1 may also actively compete with SUN2 for a limited pool of nesprin-2G, thus limiting the formation of SUN2-nesprin-2G complexes. This idea is supported

by the reduced nesprin-2–mediated actomyosin tension on the nuclear envelope measured in HGPS fibroblasts (37).

Although SUN1 is up-regulated in fibroblasts from aged individuals, this does not seem to be due to up-regulated progerin expression. We did not find a strong correlation between age and progerin expression in fibroblasts from normal individuals, consistent with a previous report (5). This suggests either that the aged cells are more sensitive to the deleterious effects of progerin (5) or that other age-related factors may enhance SUN1 accumulation.

We identify microtubules as a contributing factor to the cell polarity defects induced by progerin. Excessive microtubule coupling to the nucleus prevents its movement by actin and may also cause the actin flow phenotypes. The role of the microtubule cytoskeleton in HGPS is largely unexplored, although inhibition of the histone acetylase NAT10 appears to ameliorate nuclear defects in HGPS fibroblasts by reorganizing microtubules (38). Combined with our results, this suggests that targeting the microtubule cytoskeleton may be a possible treatment for HGPS.

It has been an ongoing debate whether the study of HGPS is relevant to our understanding of physiological aging (39, 40). Our findings strongly support the idea that at least some cellular and molecular defects in HGPS are shared with physiological aging. We observed both similar cellular defects and underlying molecular alterations in HGPS fibroblasts and fibroblasts from aged individuals. As other markers of aging do not correlate with the cell polarity defect, it is possible that the imbalance in the LINC complexes and/or the cell polarity defects precedes some of them. For example, the LINC complex has been implicated in DNA repair (41), and defects in DNA repair and other chromatin markers are dependent on progerin expression in HGPS and normal aged cells (5). Future research may determine whether there is a relationship between LINC complex imbalance, cell polarization defects, and chromatin alterations in aging.

Materials and Methods

Primary fibroblasts were from Coriell Cell Repositories and The Progeria Research Foundation. The nuclear movement assay, actin flow analysis, and FRAP analysis were performed as previously described (18, 26). Other materials and experimental details are described in *SI Appendix, Supplemental Materials and Methods*.

ACKNOWLEDGMENTS. This research was supported by NIH Grants GM099481 (to G.G.G.) and AR068636 (to G.G.G. and H.J.W.).

1. De Sandre-Giovannoli A, et al. (2003) Lamin a truncation in Hutchinson-Gilford progeria. *Science* 300:2055.
2. Eriksson M, et al. (2003) Recurrent de novo point mutations in lamin A cause Hutchinson-Gilford progeria syndrome. *Nature* 423:293–298.
3. Young SG, Meta M, Yang SH, Fong LG (2006) Prelamin A farnesylation and progeroid syndromes. *J Biol Chem* 281:39741–39745.
4. Goldman RD, et al. (2004) Accumulation of mutant lamin A causes progressive changes in nuclear architecture in Hutchinson-Gilford progeria syndrome. *Proc Natl Acad Sci USA* 101:8963–8968.
5. Scaffidi P, Misteli T (2006) Lamin A-dependent nuclear defects in human aging. *Science* 312:1059–1063.
6. Wang Y, et al. (2012) Blocking farnesylation of the prelamin A variant in Hutchinson-Gilford progeria syndrome alters the distribution of A-type lamins. *Nucleus* 3: 452–462.
7. Verstraeten VL, Ji JY, Cummings KS, Lee RT, Lammerding J (2008) Increased mechanosensitivity and nuclear stiffness in Hutchinson-Gilford progeria cells: Effects of farnesyltransferase inhibitors. *Aging Cell* 7:383–393.
8. Vidak S, Foisner R (2016) Molecular insights into the premature aging disease progeria. *Histochem Cell Biol* 145:401–417.
9. Kubben N, Misteli T (2017) Shared molecular and cellular mechanisms of premature ageing and ageing-associated diseases. *Nat Rev Mol Cell Biol* 18:595–609.
10. Serebryannyy L, Misteli T (2018) Protein sequestration at the nuclear periphery as a potential regulatory mechanism in premature aging. *J Cell Biol* 217:21–37.
11. Starr DA, Fridolfsson HN (2010) Interactions between nuclei and the cytoskeleton are mediated by SUN-KASH nuclear-envelope bridges. *Annu Rev Cell Dev Biol* 26:421–444.
12. Chang W, Worman HJ, Gundersen GG (2015) Accessorizing and anchoring the LINC complex for multifunctionality. *J Cell Biol* 208:11–22.
13. Gundersen GG, Worman HJ (2013) Nuclear positioning. *Cell* 152:1376–1389.
14. Kirby TJ, Lammerding J (2018) Emerging views of the nucleus as a cellular mechanosensor. *Nat Cell Biol* 20:373–381.
15. Lei K, et al. (2012) Inner nuclear envelope proteins SUN1 and SUN2 play a prominent role in the DNA damage response. *Curr Biol* 22:1609–1615.
16. Hiraoka Y, Dernburg AF (2009) The SUN rises on meiotic chromosome dynamics. *Dev Cell* 17:598–605.
17. Crisp M, et al. (2006) Coupling of the nucleus and cytoplasm: Role of the LINC complex. *J Cell Biol* 172:41–53.
18. Östlund C, et al. (2009) Dynamics and molecular interactions of linker of nucleoskeleton and cytoskeleton (LINC) complex proteins. *J Cell Sci* 122:4099–4108.
19. Folker ES, Östlund C, Luxton GW, Worman HJ, Gundersen GG (2011) Lamin A variants that cause striated muscle disease are defective in anchoring transmembrane actin-associated nuclear lines for nuclear movement. *Proc Natl Acad Sci USA* 108:131–136.
20. Chen ZJ, et al. (2014) Dysregulated interactions between lamin A and SUN1 induce abnormalities in the nuclear envelope and endoplasmic reticulum in progeric laminopathies. *J Cell Sci* 127:1792–1804.
21. Chen CY, et al. (2012) Accumulation of the inner nuclear envelope protein Sun1 is pathogenic in progeric and dystrophic laminopathies. *Cell* 149:565–577.
22. Zhu R, Antoku S, Gundersen GG (2017) Centrifugal displacement of nuclei reveals multiple LINC complex mechanisms for homeostatic nuclear positioning. *Curr Biol* 27: 3097–3110e5.
23. Wilson KL, Foisner R (2010) Lamin-binding proteins. *Cold Spring Harb Perspect Biol* 2: a000554.
24. Saunders CA, et al. (2017) TorsinA controls TAN line assembly and the retrograde flow of dorsal perinuclear actin cables during rearward nuclear movement. *J Cell Biol* 216: 657–674.
25. Luxton GW, Gomes ER, Folker ES, Vintinner E, Gundersen GG (2010) Linear arrays of nuclear envelope proteins harness retrograde actin flow for nuclear movement. *Science* 329:956–959.
26. Chang W, Folker ES, Worman HJ, Gundersen GG (2013) Emerin organizes actin flow for nuclear movement and centrosome orientation in migrating fibroblasts. *Mol Biol Cell* 24:3869–3880.
27. Chang W, Antoku S, Östlund C, Worman HJ, Gundersen GG (2015) Linker of nucleoskeleton and cytoskeleton (LINC) complex-mediated actin-dependent nuclear positioning orients centrosomes in migrating myoblasts. *Nucleus* 6:77–88.
28. Pacheco LM, et al. (2014) Progerin expression disrupts critical adult stem cell functions involved in tissue repair. *Aging (Albany NY)* 6:1049–1063.
29. Gomes ER, Jani S, Gundersen GG (2005) Nuclear movement regulated by Cdc42, MRCK, myosin, and actin flow establishes MTOC polarization in migrating cells. *Cell* 121:451–463.
30. Capell BC, et al. (2005) Inhibiting farnesylation of progerin prevents the characteristic nuclear blebbing of Hutchinson-Gilford progeria syndrome. *Proc Natl Acad Sci USA* 102:12879–12884.
31. Pienta KJ, Coffey DS (1990) Characterization of the subtypes of cell motility in ageing human skin fibroblasts. *Mech Ageing Dev* 56:99–105.
32. Muggleton-Harris AL, Reisert PS, Burghoff RL (1982) In vitro characterization of response to stimulus (wounding) with regard to ageing in human skin fibroblasts. *Mech Ageing Dev* 19:37–43.
33. Ridley AJ, Hall A (1992) The small GTP-binding protein rho regulates the assembly of focal adhesions and actin stress fibers in response to growth factors. *Cell* 70:389–399.
34. López-Otín C, Blasco MA, Partridge L, Serrano M, Kroemer G (2013) The hallmarks of aging. *Cell* 153:1194–1217.
35. White RR, Vijg J (2016) Do DNA double-strand breaks drive aging? *Mol Cell* 63: 729–738.
36. Campanale JP, Sun TY, Montell DJ (2017) Development and dynamics of cell polarity at a glance. *J Cell Sci* 130:1201–1207.
37. Arsenovic PT, et al. (2016) Nesprin-2G, a component of the nuclear LINC complex, is subject to myosin-dependent tension. *Biophys J* 110:34–43.
38. Larrieu D, Britton S, Demir M, Rodriguez R, Jackson SP (2014) Chemical inhibition of NAT10 corrects defects of laminopathic cells. *Science* 344:527–532.
39. Burtner CR, Kennedy BK (2010) Progeria syndromes and ageing: What is the connection? *Nat Rev Mol Cell Biol* 11:567–578.
40. Dreesen O, Stewart CL (2011) Accelerated aging syndromes: Are they relevant to normal human aging? *Aging (Albany NY)* 3:889–895.
41. Lottersberger F, Karssemeijer RA, Dimitrova N, de Lange T (2015) 53BP1 and the LINC complex promote microtubule-dependent DSB mobility and DNA repair. *Cell* 163: 880–893.

Supplemental material and methods

Reagents

LPA was from Avanti Polar Lipids (Alabaster, AL). Dye-conjugated phalloidin was from Thermo Fisher Scientific (Waltham, MA). Unless noted, all other chemicals were from Sigma-Aldrich (St. Louis, MO). Lifeact-mCherry, EGFP-mN2G, EGFP-SUN1, EGFP-SUN2, EGFP-lamin A, EGFP-progerin, EGFP-progerin-SSIM, EGFP-emerin and EGFP-LAP1 were previously described (1-4). Dr. Arnoud Sonnenberg (Netherlands Cancer Institute, Amsterdam, Netherlands) provided EGFP-tagged nesprin-3α and nesprin-3β cDNA constructs and Dr. Kyle J. Roux (Sanford Children's Health Research Center, Sioux Falls, SD) provided a EGFP-nesprin-4 cDNA construct. EGFP-lamin B1 cDNA was cloned into pEEGFP-C1p, RFP-tagged lamin A and progerin cDNAs into RFP-C1 and Myc-tagged SUN1 and SUN2 cDNA into pMSCV vector. Pericentrin mouse and rabbit antibodies were from BD Transduction Laboratories (San Jose, CA) and Covance (Princeton, NJ), respectively. Tyrosinated α-tubulin rat monoclonal antibody (YL1/2) was from the European Collection of Animal Cell Cultures (Salisbury, UK). β-actin (clone C4) mouse antibody, c-myc rabbit antibody and lamin A/C rabbit antibody were from Santa Cruz Biotechnology (Santa Cruz, CA). Lamin A/C mouse antibody (MANLAC1) was from Dr. Glenn Morris (MDA Monoclonal Antibody Resource at the Wolfson Centre for Inherited Neuromuscular Disease, Oswestry, UK). SUN1 rabbit antibody was provided by Dr. Sue Shackleton (University of Leicester, UK), as well as from Sigma-Aldrich and Abcam (Cambridge, MA). Dr. Brian Burke (Institute of Medical Biology, Singapore) provided SUN1 mouse antibody. SUN2 and γH2AX rabbit antibodies were from Abcam. HDJ-2 mouse antibody was from Lab Vision (Fremont, CA). GAPDH mouse antibody was from Ambion (Austin, TX). Progerin mouse antibody was from Abcam. GFP chicken antibody was from Millipore Sigma (Burlington, MA). Myc mouse antibody was from Sigma-Aldrich. All secondary antibodies were from Jackson ImmunoResearch (West Grove, PA). Ultra-sensitive enhanced chemiluminescent HRP substrate was from Thermo Fisher Scientific.

Cell culture and drug treatment

Serum-free medium (SFM) is Dulbecco's modified Eagle medium (Corning, Oneonta, NY) containing 10 mM HEPES (pH 7.4), penicillin and streptomycin (Thermo Fisher Scientific). NIH3T3 fibroblasts were from ATCC (Manassas, VA) and were cultured in SFM with 10% calf serum (Gemini, West Sacramento, CA). HEK293T cells (ATCC) and all human fibroblasts (Coriell Cell Repositories, Camden, NJ or The Progeria Research Foundation, Peabody, MA) were cultured in SFM with 15% fetal bovine serum (Gemini). NIH3T3 and human fibroblasts were only used for 6-8 passages except when the effect of passage on nuclear movement and senescence was tested. To serum starve cells, confluent monolayers were washed three times with SFM and maintained in SFM for 2 (NIH3T3) or 3 d (human fibroblasts). Serum-starved cells were wounded and nuclear movement was stimulated with 10 μM LPA for 45 min to detect TAN lines or 2 h to measure nuclear movement and centrosome orientation. FTI-277, when added, was used at 2.5 μM and the medium was changed daily. FTI-227 treatments were 48 h for nuclear movement assays and 72 h for FRAP assays.

Transfection and infection

For live cell imaging, plasmid DNA (10 μg/ml) diluted in 140 mM KCl, 10 mM HEPES (pH 7.4) was pressure microinjected into nuclei of cells at the wounded edge of monolayer cultures and allowed to express for 1 h before adding 20 μM LPA to stimulate nuclear movement. siRNAs (siScramble: UUCUCCGAACGUGUCACGU; siSUN1-1: CAAUCAGUGCGGUUGGUGA; siSUN1-1: GAAACUUACGAAACCAAAA; siSUN2: GGAAAUCCAGCAACAUGAA) were from

Shanghai GenePharma Co., Ltd (Shanghai, China) and were transfected at 20 μM using Lipofectamine RNAiMAX (Thermo Fisher Scientific). Stable cell lines were generated by infecting cells with retrovirus, produced in HEK293T cells, in the presence of 2 μg/ml polybrene (Millipore, Billerica, MA).

FRAP

Fibroblasts were cultured on chambered cover glasses and transfected with GFP-tagged constructs using Lipofectamine PLUS (Thermo Fisher Scientific). Experiments were performed on a Zeiss LSM 510 META confocal laser scanning system (Carl Zeiss, Oberkochen, Germany) attached to a Zeiss Axiovert 200 microscope with spectral resolution of fluorescence labels using the 488 nm line with a 30mW argon laser in conjunction with a Plan-Neofluar 40x/1.3 oil objective. A selected area with same size at each nucleus was photobleached at 50% laser power (100% transmission) for 2 iterations and the fluorescence recovery was monitored by scanning at low power (2.1% transmission) in 3 s intervals for the first 30 micrographs and 5 or 8 s intervals for another 70 micrographs. We also performed FRAP using a Nikon A1R MP multiphoton confocal microscope with imaging software NIS-Elements and environment control at 37°C and 5% CO2 (Nikon, Melville, NY). The average fluorescence intensity was measured in the region of interest and normalized to the change in total fluorescence as $I_{rel} = T_0 I_t / T_t I_0$ as described previously (2). The halftime of recovery was calculated as $t_{1/2} = ln2 \times \frac{-1}{slope}$ using data taken from the first 30 s after bleaching as reported previously (2).

Microscopy

For immunofluorescence microscopy, cells on coverslips were fixed in 4% paraformaldehyde (Electron Microscopy Sciences, Hatfield, PA), permeabilized in phosphate-buffered saline containing 5% normal goat serum and 0.3% Triton X-100 and stained with standard techniques. Coverslips were mounted with Fluoromount-G (Southern Biotech, Birmingham, AL). Fluorescence and phase contrast images were acquired with either a 40X PlanApo objective (NA 1.0) and a CoolSNAP HQ CCD camera on a Nikon TE300 inverted microscope controlled by Metamorph (Molecular Devices, Sunnyvale, CA), or with a Zeiss LSM 510 META confocal laser scanning system attached to a Zeiss Axiovert 200 inverted microscope. Movies of live cell fluorescent proteins were acquired at 37˚C (5 min per frame) with a 60X PlanApo objective (NA 1.49) and an iXon X3 CCD camera on a Nikon Eclipse Ti microscope controlled by NIS-Elements. Microscopic images and movies were processed using Fiji (5).

Data analysis

Nuclear and centrosomal positions were measured using CellPlot as previously described (6) and analyzed and plotted using Excel (Microsoft, Redmond, WA). The velocities of actin retrograde flow were calculated from the slopes of lines in kymographs generated using NIS-Elements and Fiji as previously described (7). We developed custom software (available upon request) to quantify background-subtracted immunofluorescence staining of nuclear proteins (in Fig. 5B). Quantification of immunoblot signals was done using Fiji with background subtraction. Statistical analysis was performed in Microsoft Excel. Unpaired two-tailed Student's t-tests were used to calculate p values. The trend line in Fig. 6D was the logistic regression curve fitted to the results from male fibroblasts, with 0 assigned to centrosome orientation values < 50% and 1 for values ≥ 50%. The probabilities of failed centrosome orientation (p) were calculated from the fit curve and normalized to the range of centrosome orientation values using the equation: $min \times p + max \times (1 - p)$. Here min is the average of 10 lowest values and max is the average of 10 highest values.

References

1. Luxton GW, Gomes ER, Folker ES, Vintinner E, & Gundersen GG (2010) Linear arrays of nuclear envelope proteins harness retrograde actin flow for nuclear movement. *Science* 329(5994):956-959.

2. Östlund C*, et al.* (2009) Dynamics and molecular interactions of linker of nucleoskeleton and cytoskeleton (LINC) complex proteins. *J Cell Sci* 122(Pt 22):4099-4108.

3. Wang Y*, et al.* (2012) Blocking farnesylation of the prelamin A variant in Hutchinson-Gilford progeria syndrome alters the distribution of A-type lamins. *Nucleus* 3(5):452-462.

4. Meinke P*, et al.* (2014) Muscular dystrophy-associated SUN1 and SUN2 variants disrupt nuclear-cytoskeletal connections and myonuclear organization. *PLoS Genet* 10(9):e1004605.

5. Schindelin J*, et al.* (2012) Fiji: an open-source platform for biological-image analysis. *Nat Methods* 9(7):676-682.

6. Chang W, Antoku S, & Gundersen GG (2016) Wound-healing assays to study mechanisms of nuclear movement in fibroblasts and myoblasts. *Methods Mol Biol* 1411:255-267.

7. Chang W, Folker ES, Worman HJ, & Gundersen GG (2013) Emerin organizes actin flow for nuclear movement and centrosome orientation in migrating fibroblasts. *Mol Biol Cell* 24(24):3869-3880.

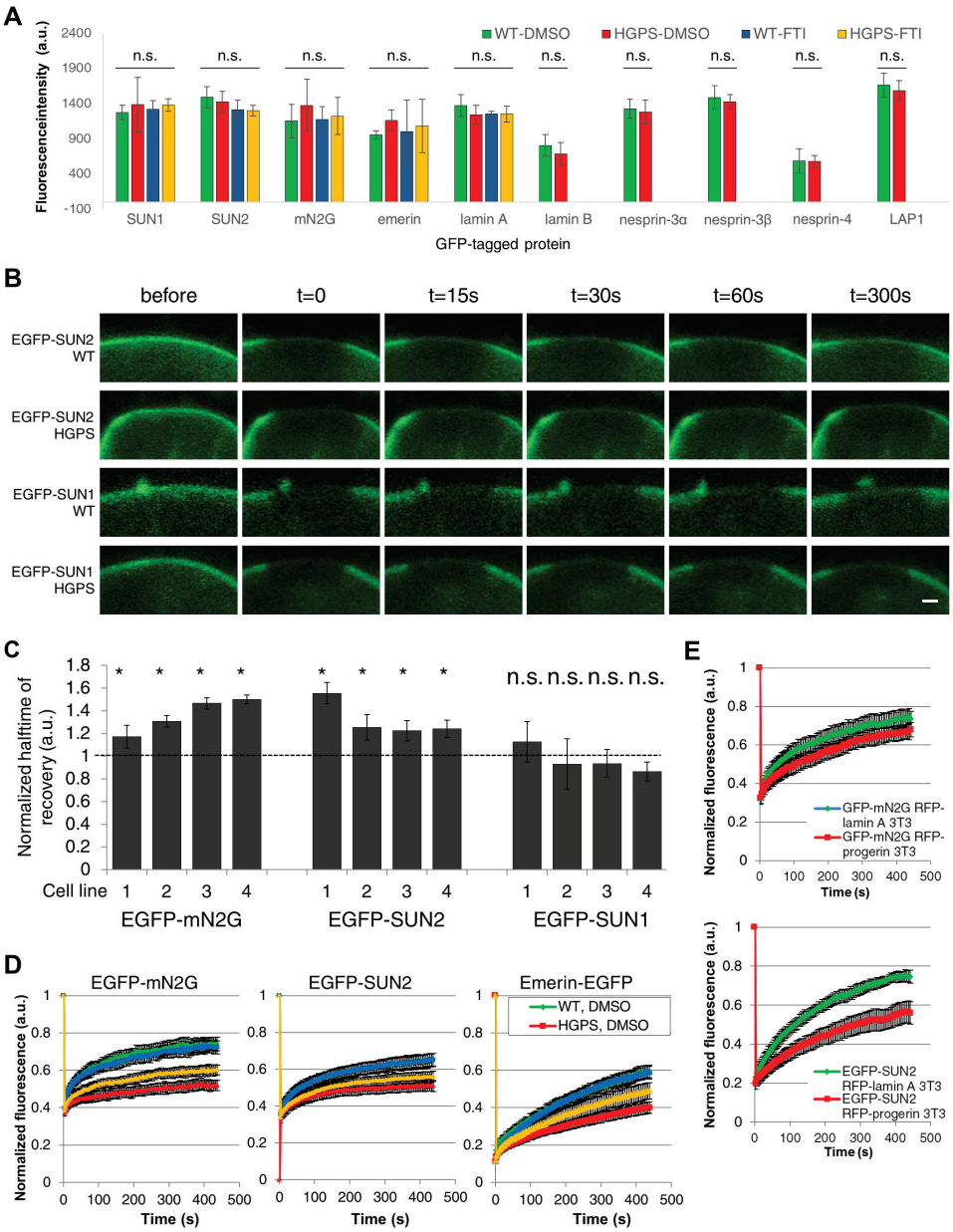

Fig. S1. Progerin expression reduces the diffusional mobilities of a subset of nuclear envelope proteins.
(A) Quantification of GFP intensities in cell used in FRAP experiments. n.s. $p > 0.05$ by one-way ANOVA test (from SUN1 to lamin A, 3 experiments, $n > 50$ cells) or by Student's t-test (from lamin B to LAP1, 3 experiments, $n > 30$ cells). *(B)* Representative images of nuclei from WT and HGPS fibroblasts expressing either EGFP-SUN2 or EGFP-SUN1 before and at the indicated times after photobleaching. Bar, 1 µm. *(C)* Normalized $t_{1/2}$ of FRAP of EGFP-tagged mN2G, SUN2, and SUN1 in four pairs of HGPS fibroblasts and sex- and age-matched controls. Statistical tests were versus controls. See Table S3 for absolute numbers. *(D)* Normalized fluorescence recovery after photobleaching for EGFP-tagged proteins in nuclei of normal fibroblasts (WT: green, DMSO-treated; blue, FTI-treated) and HGPS fibroblasts (HGPS: red, DMSO-treated; orange, FTI-treated). Cells were treated with either DMSO or 2.5 µM FTI-277 for 72 h before FRAP. *(E)* Normalized fluorescence recovery after photobleaching for EGFP-mN2G and EGFP-SUN2 in nuclei of NIH3T3 fibroblasts expressing RFP-tagged lamin A (green) or progerin (red). Data are represented as the mean ± SEM from ≥ 3 experiments ($n > 15$ cells).

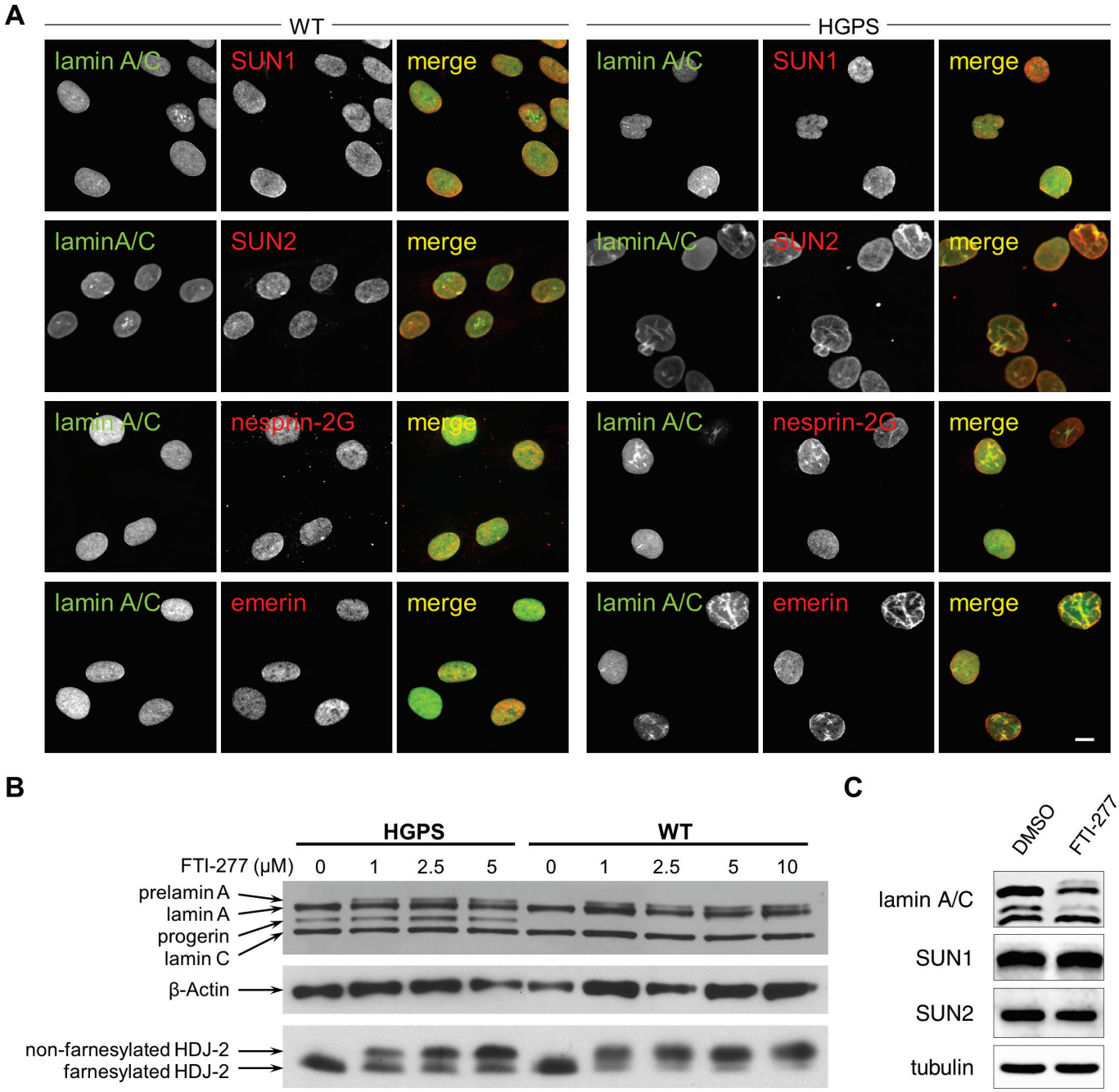

Fig. S2. Localization of emerin, nesprin-2G, SUN1, and SUN2 are similar in control and HGPS fibroblasts and FTI-277 blocks protein farnesylation.
(A) Micrographs showing immunofluorescence labeling of lamin A/C, SUN1, SUN2, nesprin-2G (N2G) and emerin in fibroblasts from a control individual (WT) and an individual with HGPS. Bar, 10 μm. *(B)* Immunoblot showing that increasing concentrations of FTI-277 interfered with prelamin A processing and caused accumulation of prelamin A in HGPS and control (WT) fibroblasts (top). β-actin (middle) is a loading control. HDJ-2 (bottom) is another farnesylation substrate and migrates slower when it is non-farnesylated. *(C)* Immunoblot showing that the levels of SUN proteins are not affected by 48 hours of FTI treatment.

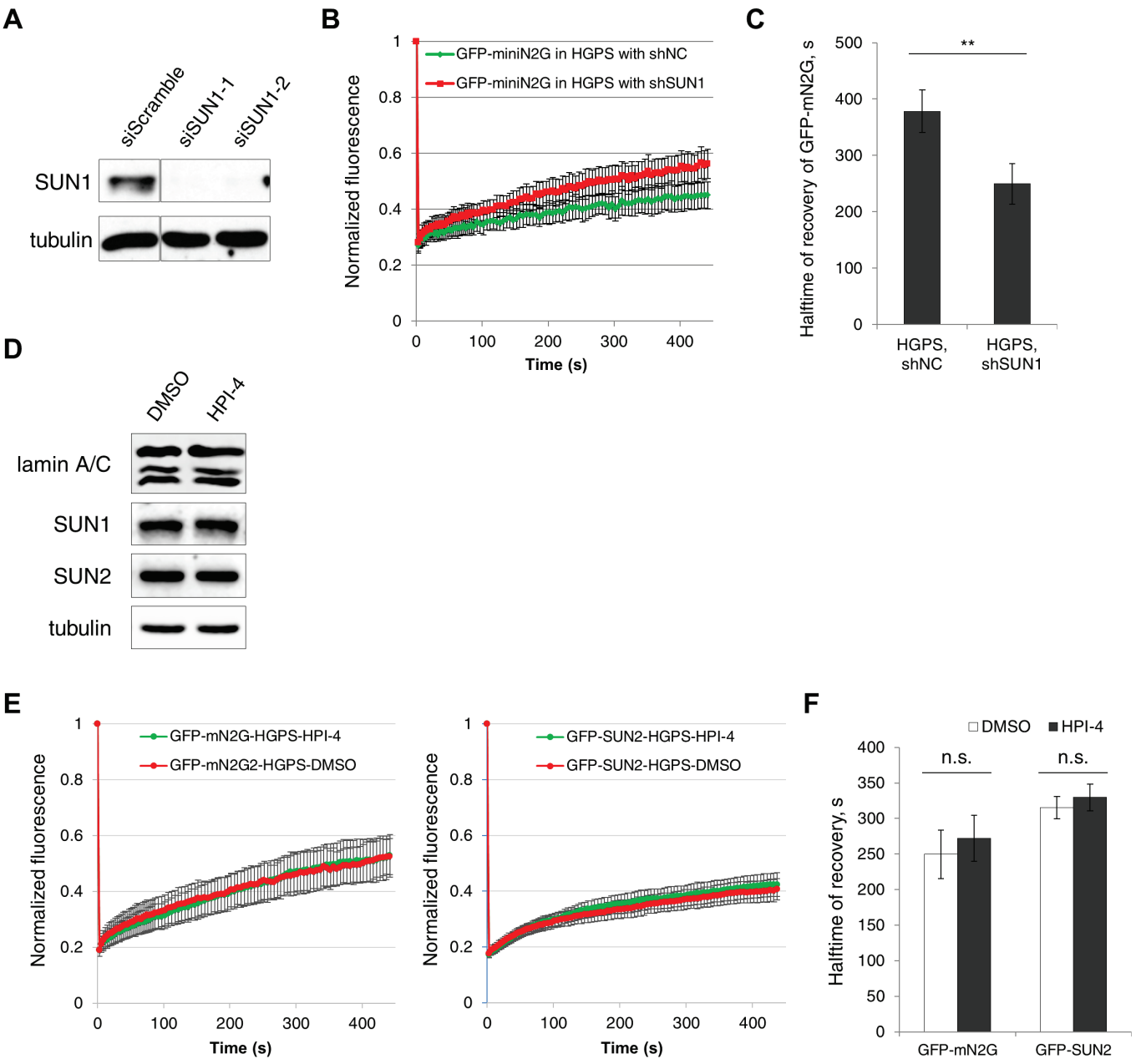

Fig. S3. SUN1 Depletion increased diffusional mobility of GFP-mN2G in HGPS fibroblasts. *(A)* Immunoblot showing that two distinct SUN1 siRNAs efficiently depleted SUN1 in human fibroblasts. Tubulin is a loading control. *(B)* Normalized FRAP for EGFP-mN2G in HGPS fibroblasts expressing control (shNC, green) and SUN1 specific (shSUN1, red) shRNAs (*N* = 3 experiments, *n* > 15 cells). *(C)* The $t_{1/2}$ of EGFP-mN2G for data in B. *(D)* Immunoblot showing that the levels of SUN proteins are not affected by 3 hours of 10 μM HPI-4 treatment. *(E)* Normalized FRAP for EGFP-mN2G and EGFP-SUN2 in HGPS fibroblasts treated with DMSO or 10 μM HPI-4. (*N* = 3 experiments, *n* > 15 cells). *(F)* The $t_{1/2}$ of EGFP-tagged proteins for data in E. n.s. p>0.05; ***p* < 0.01 by Student's t-test. Data are represented as the mean ± SEM.

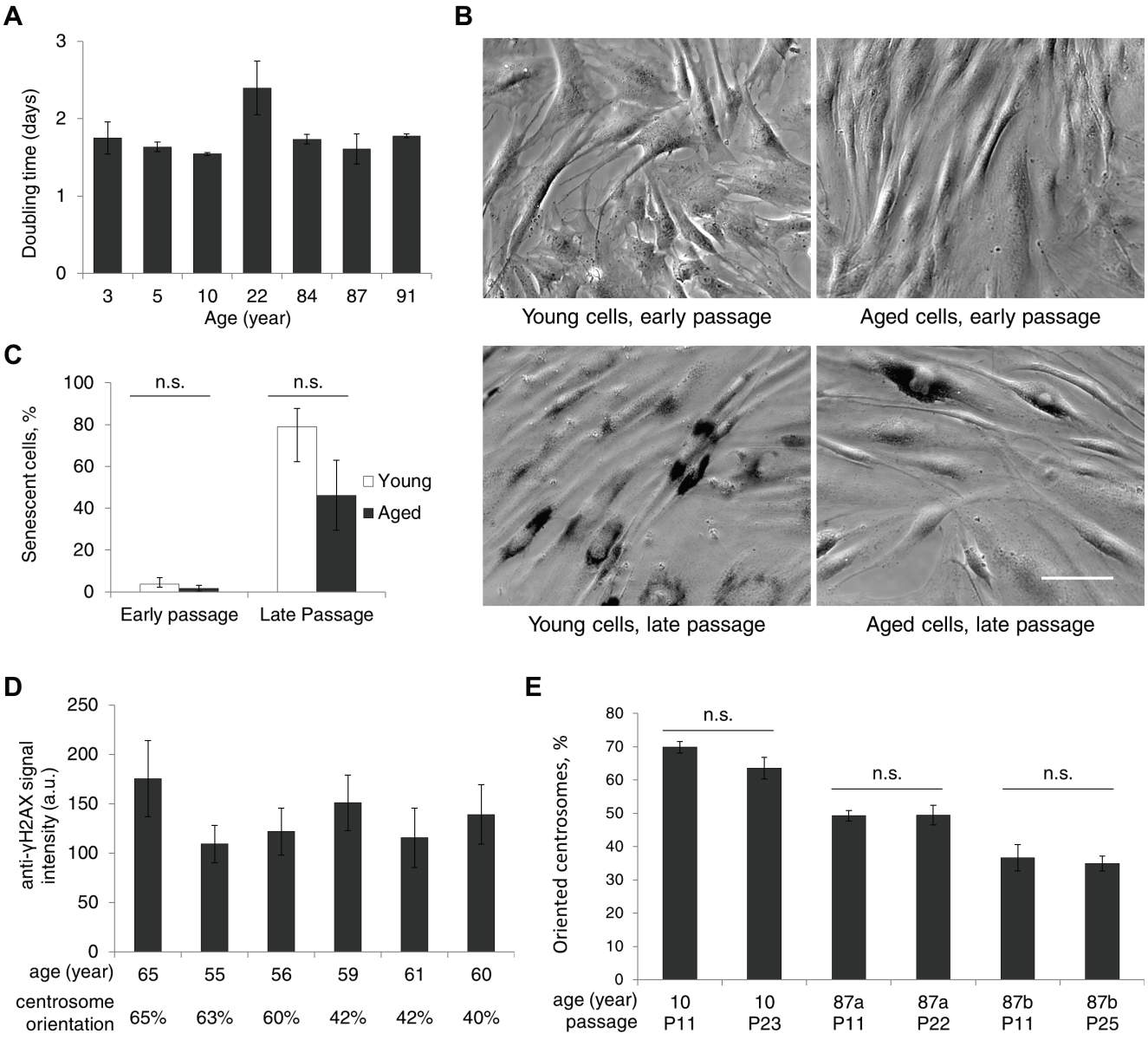

Fig. S4. Cell polarity defects in fibroblasts from aged individuals do not correlate with proliferation, senescence or DNA damage.

(A) Growth rates of fibroblasts from individuals vary without clear correlation with their ages of sampling. The fibroblasts from young and aged individuals used in nuclear movement assays exhibited similar growth rates, as measured by doubling times. There was no significant difference in growth rates between young (3-10) and old (84-91) fibroblasts by t-test (*N* = 2 experiments). *(B)* Representative images of early (≤ 15) and late (> 20) passages of fibroblasts from both young and aged individuals stained for senescence β-galactosidase activity (black staining). Bar, 50 μm. *(C)* Quantification of cellular senescence for the cells shown in B. (*N* = 3 experiments, *n* > 150 cells). *(D)* Quantification of DNA double strand breaks as measured by γH2AX signal in fibroblasts from six individuals with similar ages at sampling (*n* > 150 cells). The level of centrosome orientation is shown below. Student's t-test showed that there was no significant difference between fibroblasts with normal (left three) compared to defective (right three) centrosome orientation ($p > 0.99$). *(E)* Centrosome orientation was similar at early and late passage in fibroblasts from either young or aged individuals. (*N* = 2 experiments, *n* > 150 cells). Data are represented as the mean ± SEM. n.s. $p > 0.05$ by Student's t-test.

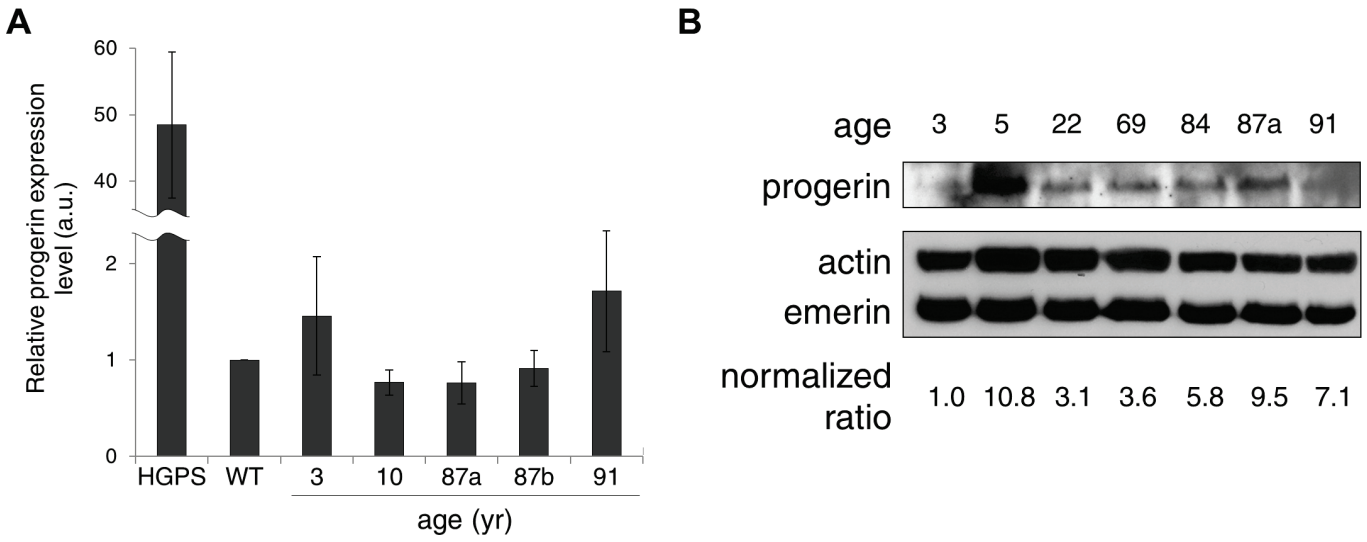

Fig. S5. Progerin level in fibroblast do not correlate with age.
(A) Quantification of progerin mRNA in dermal fibroblasts from young and aged individuals by RT-PCR. Fibroblasts from a subject with HGPS served as a positive control. There is no significant difference in progerin mRNA levels in fibroblasts from young and aged individuals by t-test. Error bars, SEM from n = 3 measurements. (B) Progerin protein (top) was detected in whole cell lysates (see Methods) of fibroblasts from both young and aged individuals. Actin and emerin (bottom) served as loading control. The ratio is progerin/actin normalized to first sample.

Supplemental tables

Table S1. Pairs of dermal fibroblast lines from control individuals (WT) and children with HGPS.

Name	ID	Sex	Age (yr)	Source	Note
WT1	GM00316	male	12	CCR*	
HGPS1	AG11498	male	14	CCR	
WT2	GM00498	male	3	CCR	
HGPS2	AG06917	male	3	CCR	
WT3	GM01652	female	11	CCR	
HGPS3	AG01972	female	14	CCR	
WT4	GM00038	female	9	CCR	
HGPS4	AG11513	female	8	CCR	
WT5	HGFDFN 168	male	40	PRF†	father of HGADFN 167
HGPS5	HGADFN 167	male	8	PRF	son of HGFDFN 168
WT6	HGMDFN 371	female	45	PRF	mother of HGMDFN 370
HGPS6	HGADFN 370	female	10	PRF	daughter of HGMDFN 371

* CCR: Coriell Cell Repositories
† PRF: Progeria Research Foundation

Table S2. Summary of $t_{1/2}$ in FRAP experiments (Figure 1).

EGFP-tagged protein	Treatment	$t_{1/2}$ (s)*	
		WT	**HGPS**
Figure 1A			
lamin A		343.4 ± 30.3	462.5 ± 43.1
lamin B1		565.6 ± 64.2	612.9 ± 62.9
SUN2		147.9 ± 12.8	191.8 ± 7.6
SUN1		184.7 ± 14.0	196.9 ± 20.6
mN2G		87.8 ± 4.9	127.8 ± 8.2
nesprin-3α		197.2 ± 9.8	228.8 ± 21.3
nesprin-3β		130.0 ± 16.8	153.8 ± 16.7
nesprin-4		171.5 ± 10.6	190.6 ± 10.7
Emerin		185.5 ± 11.6	269.0 ± 18.7
LAP1		161.2 ± 10.0	183.8 ± 14.3
Figure 1B			
SUN2	DMSO	147.2 ± 9.8	196.8 ± 10.9
SUN2	FTI-277	134.8 ± 6.2	164.3 ± 8.3
mN2G	DMSO	86.3 ± 10.2	184.1 ± 12.8
mN2G	FTI-277	94.5 ± 10.0	142.2 ± 11.0
Emerin	DMSO	185.5 ± 11.6	269.0 ± 10.0
Emerin	FTI-277	169.5 ± 11.6	210.1 ± 7.6
EGFP-tagged protein		**NIH3T3 expressing RFP-lamin A**	**NIH3T3 expressing RFP-progerin**
Figure 1C			
SUN2		159.1 ± 11.1	260.6 ± 19.7
mN2G		94.5 ± 12.2	148.6 ± 18.5

* $t_{1/2}$ is expressed as means ± standard errors from ≥ 3 experiments (n > 15 cells).

Table S3. Summary of $t_{1/2}$ in fibroblasts derived from matched controls (WT) and subjects with HGPS for FRAP experiments (Figure S1C).

Cell lines	$t_{1/2}$ (s)* EGFP-SUN2	$t_{1/2}$ (s) EGFP-SUN1	$t_{1/2}$ (s) EGFP-mN2G
WT1	112.7 ± 13.5	178.1 ± 25.2	79.2 ± 9.3
HGPS1	175.3 ± 10.5	200.7 ± 31.6	92.9 ± 7.8
WT2	138.2 ± 18.5	174.6 ± 17.7	88.2 ± 5.8
HGPS2	173.3 ± 15.7	162.2 ± 39.1	115.4 ± 7.4
WT3	140.5 ± 12.5	165.1 ± 28.9	103.3 ± 7.5
HGPS3	172.2 ± 12.3	154.3 ± 20.4	151.5 ± 11.4
WT4	145.0 ± 12.5	164.3 ± 22.6	102.0 ± 5.9
HGPS4	180.0 ± 11.3	142.1 ± 13.8	153.0 ± 14.2

* $t_{1/2}$ is expressed as means ± standard errors from ≥ 3 experiments (n > 15 cells).

Table S4. Dermal fibroblasts from apparently normal men used in this study, related to Figure 6.

Strain	Catalog ID[a]	Biopsy source	Race/Ethnicity	Age at biopsy (yr)	Population doubling level at freeze	Passage frozen
3	GM05565	inguinal	Hispanic/Latino	3		5
5	GM05381	umbilical area	Black	5		3
10	GM03348	unspecified	Caucasian	10		7
12	GM00316	arm	Caucasian	12		12
17	AG06234	arm	Caucasian	17	6.5	3
22	AG11747	arm	Caucasian	22	16	
30a	AG11242	arm	Caucasian	30	9	
30b	AG13153	arm	Caucasian	30	5.54	6
33	AG04438	arm	Caucasian	33	13	
44	AG13156	arm	Caucasian	44	7	3
49	AG11160	arm	Caucasian	49	6	
51	AG07136	arm	Caucasian	51	9	
55	AG12657	arm	Caucasian	55	5	2
56	AG13292	arm	Caucasian	56	5	2
59	AG06239	arm	Caucasian	59	8	
60	AG05419	arm	Caucasian	60	19	
61	AG11011	arm	Caucasian	61	7	
65	AG04659	arm	Caucasian	65	9	
68	AG16030	arm	Caucasian	68	6	3
69a	AG05095	arm	Caucasian	69	8	
69b	AG05099	arm	Caucasian	69	7	
72	AG04455	arm	Caucasian	72	9	
84a	AG05274	arm	Caucasian	84	14	
84b	AG11730	arm	Caucasian	84	5.97	4
87a	AG10884	arm	Caucasian	87	7	
87b	AG05248	arm	Caucasian	87	16	
91	AG07725	arm	Caucasian	91	11	

[a]Source: Coriell Cell Repositories.

Table S5. Dermal fibroblasts from apparently normal women used in this study, related to Figure 6D.

Catalog ID[a]	Biopsy source	Race/Ethnicity	Age at biopsy (yr)	Population doubling level at freeze	Passage frozen
GM02036	unspecified	Caucasian	11	6.21	13
GM01651	arm	Caucasian	13	7.09	11
AG11732	arm	Caucasian	24	7.11	
AG11745	arm	Caucasian	43	8	
AG11793	arm	Caucasian	48	8	
AG11564	arm	Caucasian	57	9	
AG11733	arm	Caucasian	70	8	
AG11725	arm	Caucasian	84	8	
AG09602	arm	Caucasian	92	5.48	2

[a]Source: Coriell Cell Repositories.

Description of Supplemental Movies

Movie S1
Time-lapse movie of LPA-stimulated actin cable movement in a mCherry-LifeAct and EGFP-progerin expressing NIH3T3 cell (panels presented in Fig. 3C). Wound edge is at the top. Actin cables move rearward but the nucleus is immobile. Progerin accumulates on actin cables and appears to move together with them, suggesting that the lamina with progerin cannot resist the force from actin cables and fails to transduce force to move the nucleus. Time: h:min.

Movie S2
Time-lapse movie of LPA-stimulated NIH3T3 fibroblast expressing mCherry-LifeAct and EGFP-lamin A (panels presented in Fig. 3E). Wound edge is at the top. Actin cables move rearward in an oriented fashion and their velocity is much faster than that in an EGFP-progerin expressing cell (see Movie S3). Time: h:min.

Movie S3
Time-lapse movie of LPA-stimulated NIH3T3 cell expressing mCherry-LifeAct and EGFP-progerin (panels presented in Fig. 3F). Wound edge is at the top. Actin cables move haphazardly and their velocity is slower compared to that in NIH3T3 fibroblasts expressing EGFP-lamin A (see Movie S2) or EGFP-progerin-SSIM (see Fig. 3G), indicating that progerin expression also impacts actin flow. Time: h:min.